Journal of Materials Chemistry A

ROYAL SOCIETY OF CHEMISTRY

COMMUNICATION

View Article Online
View Journal | View Issue

Open Access Article. Published on 02 October 2020. Downloaded on 12/4/2025 8:07:59 PM.
This article is licensed under a Creative Commons Attribution 3.0 Unported Licence.

Check for updates

Cite this: J. Mater. Chem. A, 2020, 8, 22001

Received 1st August 2020
Accepted 2nd October 2020

DOI: 10.1039/d0ta07544b

rsc.li/materials-a

Janus wood membranes for autonomous water transport and fog collection†

Yong Ding,[ab] Kunkun Tu,[ab] Ingo Burgert[ab] and Tobias Keplinger*[ab]

Autonomous and directional transport of liquids is crucial for many applications, ranging from microreactors to water harvesting. Particularly, Janus membranes, with asymmetric wettability on two sides, present enticing opportunities to address this challenge. With the inner driving force arising from the asymmetric wettability, Janus membranes can promote the desired transport without an external energy input. However, the elaborate bottom-up fabrication processes and poor mechanical performance of commonly employed membrane substrates often restrict their utilization, especially for engineering applications. Here, we report a wood-based Janus membrane demonstrating directional, spontaneous, and fast transport of water. Mechanically robust bio-based and renewable Janus wood membranes represent a crucial milestone towards larger-scale application of Janus membranes, for example in bilayer structures with excellent fog-capturing efficiency implemented in future smart building applications.

Autonomous directional transport of liquids has attracted great interest in the fields of microfluidic manipulation, chemical analysis, microreactors and fog collection.[1–5] It provides an energy-efficient method to direct liquid motion without an external energy supply (*e.g.* electric field) and avoids complex and expensive devices thanks to the elimination of pumps and condensers. Inspired by spider silk[6] and butterfly wings,[7] directional transport of liquids on one-dimensional (1D) fibers and two-dimensional (2D) surfaces has been widely demonstrated by the introduction of topographic and chemical gradients, individually or cooperatively.[8–13] However, the transport of liquids on fibers and surfaces suffers typically from low transport efficiency caused by a limited transport distance, low transport velocity, and liquid loss.[14–16]

Compared to open surfaces, directional liquid transport through three-dimensional (3D) porous membranes is more efficient. The liquid permeates from one side to the other, but its transport is blocked in the reverse direction. Therefore, liquid loss and long distance transport are avoided. Mostly utilized substrates include fabrics and nanofibrous membranes. Directional liquid transport within fabrics necessitates a through-plane lyophobic-to-lyophilic wettability gradient as the driving force.[17–20] Alternatively, two pieces of nanofibrous membranes with opposite wettability that are tightly stacked together reveal directional liquid transport ability due to their abrupt wettability change.[21–23] Membranes with asymmetric wettability are named after the two faces of Janus in the ancient Roman myth as Janus membranes. We briefly conclude three key elements for Janus membranes to achieve efficient directional liquid transport for engineering applications: (1) a sufficient wettability gradient across the membrane for driving the transport; (2) an internal porous structure with channels for rapid liquid transport; (3) an appropriate material substrate that balances transport efficiency and mechanical performance.

Although tremendous progress in creating wettability gradients across membranes is evident,[17–23] the applications of Janus membranes are still limited, mainly due to the employed substrates. Commonly utilized fabrics and nanofibrous based Janus membranes require elaborate and time-consuming bottom-up fabrication techniques to achieve desired pore sizes and channels for transport. In addition, the thickness of reported fabrics and nanofibrous membranes is restricted to several hundreds of micrometers, which impedes their utilization in large scale and load-bearing scenarios. As an alternative, we here propose the usage of native wood as the membrane scaffold. The unique characteristics of wood, a bio-based, renewable and mechanically robust material with a hierarchical structure, composed of well-connected hollow fibers, make it an ideal substrate for liquid transport.[24,25] However, up to now these studies do not report the utilization of native wood

[a]Wood Materials Science, Institute for Building Materials, ETH Zürich, 8093 Zürich, Switzerland. E-mail: tkeplinger@ethz.ch

[b]WoodTec Group, Cellulose & Wood Materials, EMPA, 8600 Dübendorf, Switzerland

† Electronic supplementary information (ESI) available: Methods, supplementary text, Fig. S1–S7, Tables S1 and S2, and captions for Movies S1–S3 and Movies S1–S3. See DOI: 10.1039/d0ta07544b

Open Access Article. Published on 02 October 2020. Downloaded on 12/4/2025 8:07:59 PM.
This article is licensed under a Creative Commons Attribution 3.0 Unported Licence.

for autonomous directional water transport without an additional energy input.[26–30]

Introducing a wettability gradient into wood membranes

In a simple two-step functionalization process, we equipped wood scaffolds with the necessary wettability gradient. Fig. 1 shows the fabrication and morphology of Janus wood membranes. We used time-efficient and scalable laser cutting to fabricate thin wood membranes (cross-section) and obtained smooth surfaces with open channels on both sides, which is a crucial prerequisite for creating well-defined wettability gradients and allowing a rapid liquid flow (Fig. S1, ESI†). Although conventional saw cutting or sanding is widely used for wood sample preparation, the obtained cross sectional surfaces are of poor quality and/or cell wall fragments and dust particles clog the porous structure (Fig. S2, ESI†). The obtained roughness critically affects the liquid behavior on the solid surface[31] and blocks channels, which lowers the transport efficiency. Scanning electron microscopy (SEM) images of laser-cut wood cross sections (native wood membrane) exhibited a porous structure due to cut-open wood cells (Fig. 1b, c and S3, ESI†). The surface is smooth, and all micro-channels are intact and open. These results confirm that the applied laser cutting is highly beneficial compared to previously used saw cutting in preparing thin wood membranes, especially cross sections with well-preserved surfaces for membrane applications.

The obtained native wood membranes were then immersed in fluoro-oxysilane/TiO_2 nanoparticle solution under gentle stirring and the assistance of vacuum. Benefiting from the abundant hydroxyl groups of wood scaffolds which acted as active sites for chemical modifications, a uniform silane-modified TiO_2 nanoparticle layer was deposited on the cell walls. SEM images of the modified wood scaffold surface show that the surface roughness increased compared to the native wood scaffold. The porous structure was kept open (Fig. 1d and e) and energy dispersive X-ray spectroscopy (EDXS) mapping analysis of the inner membrane structure confirmed a uniform and dense fluoro-oxysilane/TiO_2 layer without blocking the microchannels (Fig. 1h–j). Due to the hydrophobicity of fluoro-oxysilane and the nanoscale roughness from TiO_2 nanoparticles, the wettability of the wood membranes turned from hydrophilic to hydrophobic.[32]

One-side UV-irradiation treatment of the hydrophobic wood membranes was followed as a second modification step. The UV-irradiated surface became hydrophilic because of the TiO_2 induced photocatalytic decomposition of the hydrophobic silane,[33–35] whereas the unexposed surface remained hydrophobic. Since the photocatalytic silane decomposition depends on the extent of UV irradiation, the photodegradation rate within the membrane decreased gradually across the membrane thickness, thus creating a wettability gradient.[36–38] To prove the successful conversion into Janus wood membranes we performed a detailed SEM and EDXS analysis. Although the morphology of the Janus wood membrane surface did not exhibit obvious changes (Fig. 1f and g), EDXS spectra of the Janus wood membrane clearly revealed the different chemical composition of the UV-irradiated side and the unexposed side (Fig. 1k, l and S4, ESI†). While the unexposed side composition remained unaltered, the fluorine peak disappeared in the spectrum of the UV-irradiated side, which clearly confirmed the degradation of fluoro-oxysilane by UV light. The main advantage of the employed UV-irradiation technique is its simplicity, previously used to produce an in-plane wettability gradient on less complex solid surfaces like glass substrates.[32] Our results prove its effectiveness to create a through-plane wettability gradient even within a complex material such as wood.

Autonomous water transport by the wettability gradient

We then tested the water transport ability of the Janus wood membrane. Fig. 2 displays a series of still frames taken from a video during dropping water on a Janus wood membrane (12 h UV-irradiated, 1.5 mm). When water was dropped onto the hydrophobic side (the positive direction), it penetrated spontaneously to the hydrophilic side (Fig. 2a). In contrast, when water was dropped onto the hydrophilic side (the reverse direction), water transport was blocked and the droplet spread on the hydrophilic side (Movies S1 and S2, ESI†). This straightforward experiment confirms the Janus membrane's directional water transport ability, which is driven by the Laplace pressure of the curved water droplet on the asymmetrically wettable Janus membrane.[39] In addition, the hydrophilic surface induced water transport by pulling the droplet *via* a negative capillary pressure.[39] The resulting liquid transport occurred automatically, without additional energy supply.[40–42] Moreover, changing the water feeding and membrane position proved the anti-gravity autonomous transport of water within the Janus wood membranes. Fig. 2b shows a water droplet attached to the lower surface of a horizontally positioned membrane. When the hydrophobic surface was the lower side, water was transported to the upper hydrophilic surface (positive direction). When the membrane was turned (reverse direction), attaching a water droplet to the lower hydrophilic membrane side leads to water spreading on the surface and no water transport to the upper hydrophobic side. The vertically oriented Janus wood membrane also exhibited this type of water flow behavior (Movie S3, ESI†).

The water contact angle (CA) analysis of Janus wood membranes provided better understanding of the directional water transport behavior. The CA of a water drop on the Janus wood membrane in the positive direction decreased from 96° to 0° (Fig. 3a). This reduction was attributed to the permeation of the droplet through the wood membrane. It took approximately 7 seconds for the droplet to permeate completely through the wood membrane. In contrast, the water droplet CA on the reverse side decreased from 29° to 11° in 10 seconds, because the water droplet simply spread on the hydrophilic surface and finally formed a thin water film. These results confirmed that

Open Access Article. Published on 02 October 2020. Downloaded on 12/4/2025 8:07:59 PM.
This article is licensed under a Creative Commons Attribution 3.0 Unported Licence.

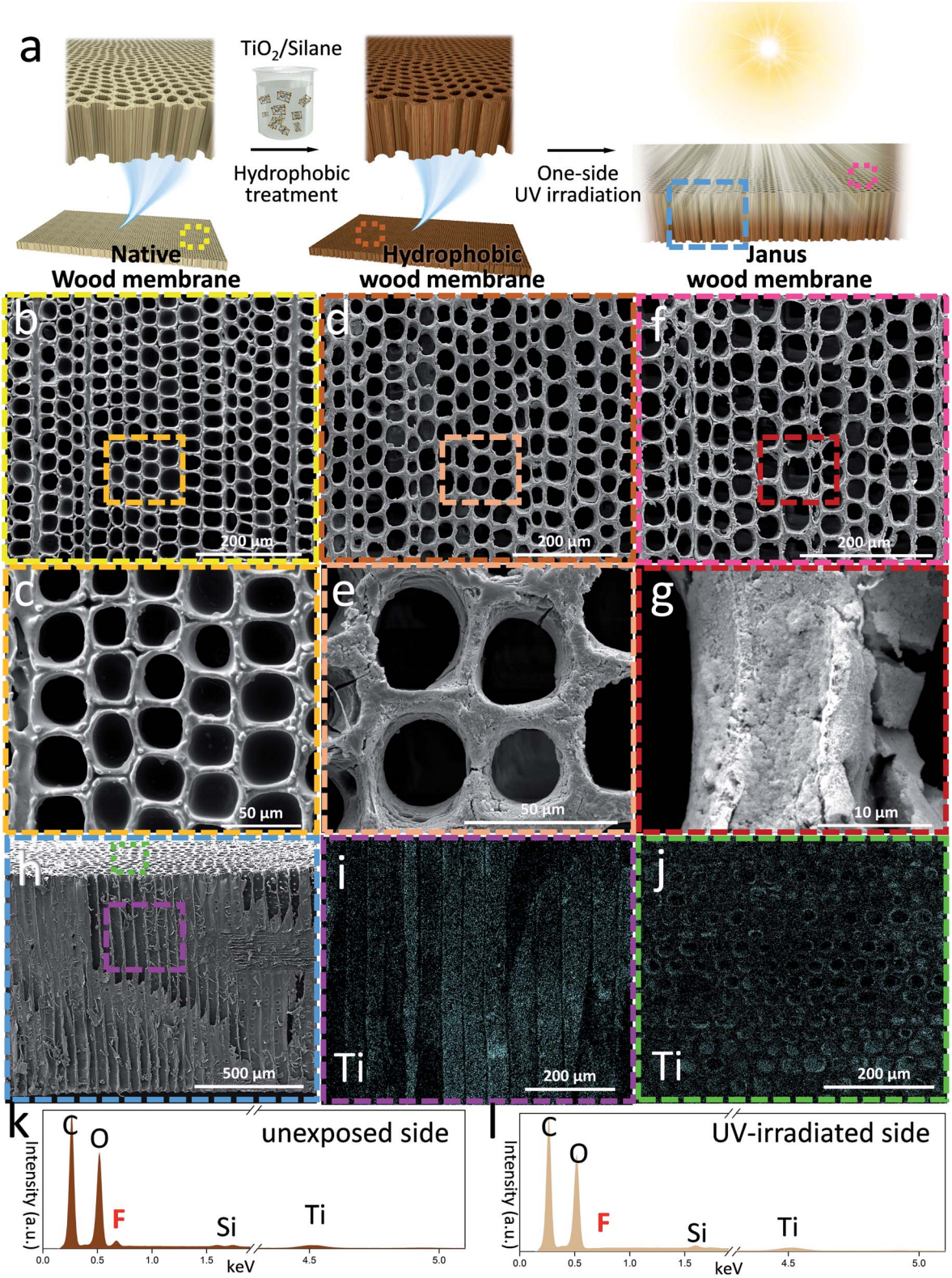

Fig. 1 Fabrication and morphology of wood membranes. (a) Illustration of the fabrication process: native wood membrane prepared by laser cutting was first modified with fluoro-oxysilane/TiO_2 nanoparticles to obtain hydrophobic membranes, and then UV irradiated on one side to create a Janus wood membrane. (b and c) SEM images of the native wood membrane. (d and e) SEM images of the hydrophobic wood membrane. (f and g) SEM images of the Janus wood membrane on the UV-irradiated side. (h) SEM image of the Janus wood membrane showing open channels and a smooth surface. (i and j) EDXS mapping image showing (i) Ti element distribution in channels and (j) Ti element distribution on the surface. (k and l) EDXS spectra obtained from the Janus wood membrane: (k) unexposed side and (l) UV-irradiated side.

Open Access Article. Published on 02 October 2020. Downloaded on 12/4/2025 8:07:59 PM.
This article is licensed under a Creative Commons Attribution 3.0 Unported Licence.

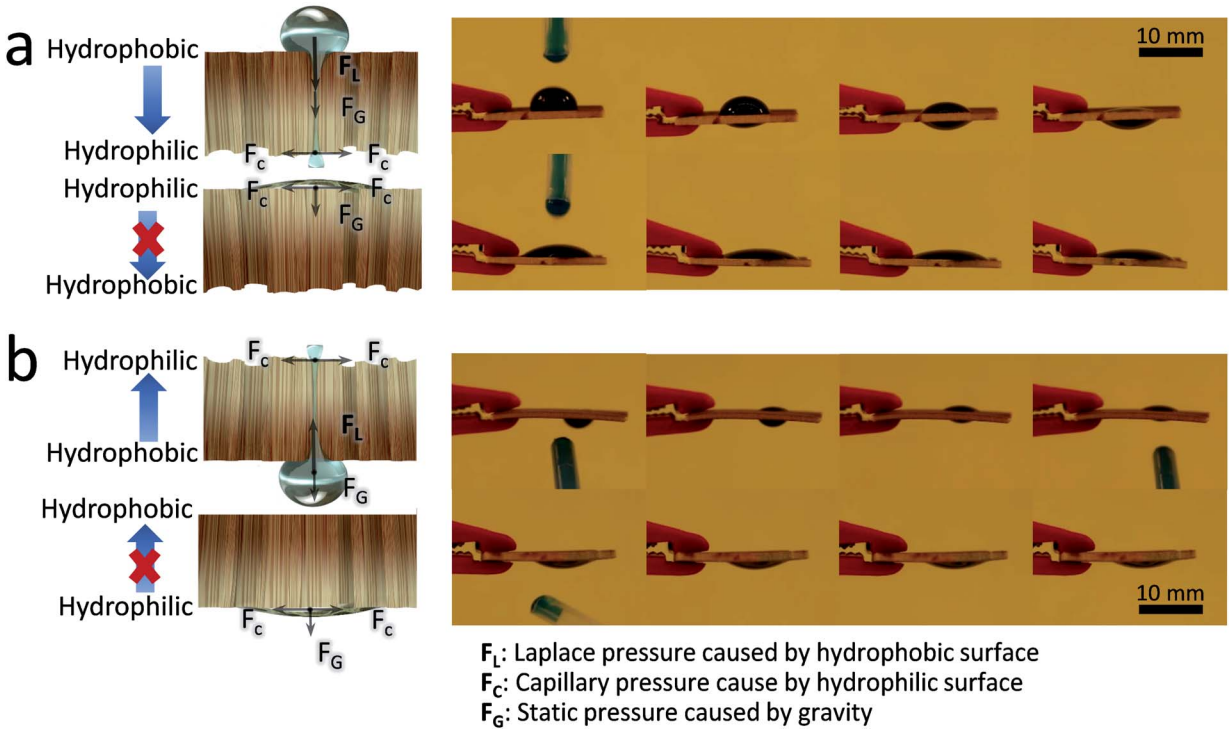

Fig. 2 Still frames taken from videos showing the dropping of water (50 μL), (a) on the horizontally oriented Janus wood membrane, first on the hydrophobic side (time interval, 2 s), and then on the hydrophilic side (time interval, 7 s). (b) Water droplet attached to the lower surface of a horizontally oriented Janus wood membrane, first on the hydrophobic side (time interval, 1.6 s) and then on the hydrophilic side (time interval, 7 s).

the wettability gradient across Janus membranes triggered the directional water transport.

The sufficient wettability gradient is indispensable for the Janus wood membrane system. For comparison, we have investigated in the following the CA of differently modified membranes. Fig. 3b shows the CA values of native-, TiO_2 nanoparticle modified-, fluoro-oxysilane modified-, and Janus wood membranes (modified with combination of TiO_2 and silane) after 12 h UV-irradiation of one side. The difference of the CA of the UV-irradiated side and unexposed side is defined as ΔCA ($\Delta CA = CA_{unexposedside} - CA_{UV\text{-}irradiatedside}$) here. ΔCA measures herewith the wood membrane wettability gradient, which acts as the driving force for the directional water transport. Wood membranes modified with TiO_2 nanoparticles revealed a limited ΔCA of 28°. The fluoro-oxysilane modified wood membrane showed a ΔCA of only 20°, because silane degraded much slower without the photocatalytic effect of TiO_2. Our Janus wood membranes modified with a combination of TiO_2 and silane possessed the highest ΔCA of 80°. Due to the photocatalytic degradation of fluoro-oxysilane by TiO_2, the UV-irradiated surface turned into hydrophilic, while the unexposed side remained hydrophobic.

With respect to the modification process, the UV-irradiation time is a crucial parameter to achieve the highest wettability gradient. As the UV irradiation time increased, the CA of the UV-irradiated side decreased rapidly from 120° to 20° at 12 h (Fig. 3c). Longer UV irradiation times of up to 24 h did not cause an obvious decrease in the CA. During UV treatment, the CA of the unexposed side decreased from 120° to 100° after the first 3 h, but remained stable at 100° as the UV irradiation time increased. For the most efficient Janus wood membrane functionalization process, we opted for 12 h as the optimum UV-irradiation time.

Janus type membranes possess a characteristic trade-off between the transport efficiency and membrane thickness. Hence, we evaluated Janus wood membranes with a thickness from 1 mm to 3 mm. According to the water droplet test, we observed that for thicker samples, it took a longer time for the water droplet to break through the wood membrane. While it took 7 seconds for water to break through a 1.5 mm-thick Janus wood membrane, it took 7 times longer time (50 seconds) for a 2 mm-thick Janus wood membrane. At a membrane thickness of more than 2.5 mm, water cannot penetrate through any side of the Janus wood membrane without the assistance of external pressure.

Directional water transport properties within Janus wood membranes are determined by two main factors: the amount of both-sided open fibers (transport path) and gradient density (driving force) (Fig. 3d). When a wood cross section is cut, some fibers are open from both ends, and these fibers allow a direct water flow, whereas other fibers are closed from one end, blocking the water flow (Fig. S6, ESI†).

Based on a simple model we calculated the probability of open fibers from both ends in the wood cross section. For 1 mm, 2 mm or 3 mm thick membranes, the probabilities to have open fibers are 66%, 33% and 0%, respectively. The second

 This journal is © The Royal Society of Chemistry 2020

Open Access Article. Published on 02 October 2020. Downloaded on 12/4/2025 8:07:59 PM.
This article is licensed under a Creative Commons Attribution 3.0 Unported Licence.

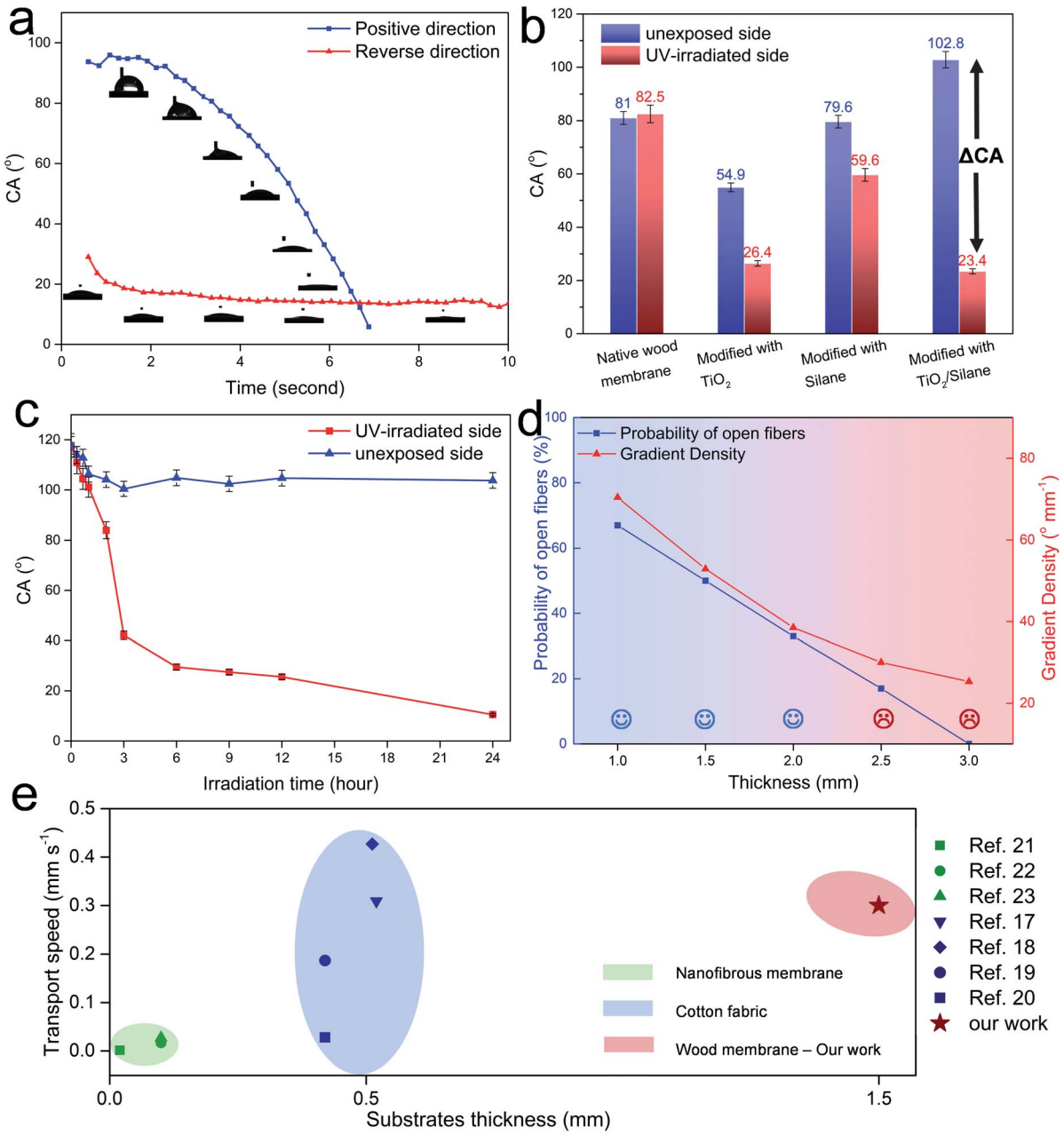

Fig. 3 (a) Change of the CA over time of a water droplet on a Janus wood membrane in positive and reverse directions. (b) CA of the native wood membrane, wood membrane modified with TiO_2 nanoparticles only, fluoro-oxysilane only, and combination of TiO_2 nanoparticles and fluoro-oxysilane. (c) CA change after UV irradiation on the UV-irradiated side and unexposed side of the Janus wood membrane. (d) Probability of open fibers and gradient density with the thickness of the Janus wood membrane. (e) Comparison of Janus wood membranes with other Janus systems.

crucial factor for the autonomous liquid transport is the gradient density, as the driving force. It is defined as ΔCA/thickness. When ΔCA remains unchanged, the gradient density decreases as the thickness increases. At a membrane thickness of 2.5 mm or higher, on one hand, the gradient density was too low to trigger the water transport (not enough driving force) and on the other hand, the probability of open pores is relatively low (not enough open transport path). For a maximum transport efficiency, 1.5 mm is the optimal thickness for Janus wood membranes.

To evaluate the performance of the developed and optimized Janus wood membranes we compared them with other existing Janus systems regarding transport velocity related to the substrate thicknesses (Fig. 3e). The thickness of electrospun polymeric nanofibrous based Janus membranes ranges from 0.02–0.1 mm and the maximally achieved water transport velocity reported is 0.03 mm s^{-1}.[21–23] Common fabric based Janus membranes have a greater thickness of approximately 0.5 mm. Their directional water transport velocity improved progressively over the last few years from 0.03 mm s^{-1} to

Open Access Article. Published on 02 October 2020. Downloaded on 12/4/2025 8:07:59 PM.
This article is licensed under a Creative Commons Attribution 3.0 Unported Licence.

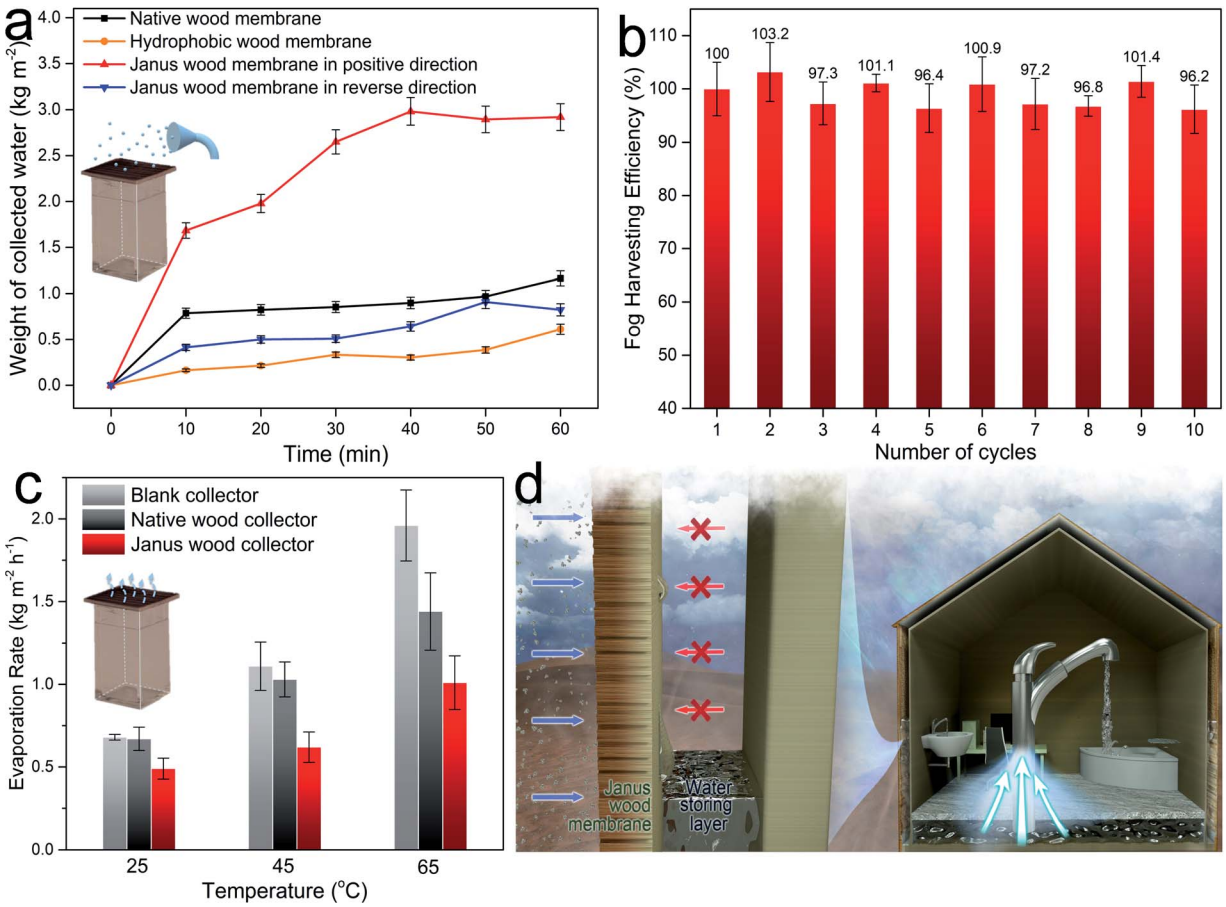

Fig. 4 Potential application of the Janus wood membrane in fog capture. (a) Illustration of the fog capture device and fog collection efficiency of designed devices. (b) Cycling test of fog harvesting efficiency. (c) Water evaporation rate at different temperatures. (d) Scheme of a potential bilayer smart building constructed with the Janus wood membrane and water storing layer.

0.4 mm s^{-1}, representing the most efficient water self-transport system to date.[17–20] In our work, we achieved a fast water transport speed of 0.3 mm s^{-1} with 1.5 mm thick membranes. Our Janus wood membranes herewith demonstrate a comparable transport efficiency to the best-performing fabric based Janus membranes with a three-times higher membrane thickness. By utilizing wood as the membrane scaffold, we benefit not only from the intrinsic transport channels, but also from an excellent mechanical performance. Janus wood membranes exhibited a compressive strength of 58 MPa (longitudinal direction) and tensile strength of 3.4 MPa in the radial direction (Fig. S7 and Table S1, ESI†).

Janus wood membrane facilitated fog harvesting for smart building

A mechanically robust Janus wood membrane with capability for fast and directional water transport opens up an avenue for various applications. One promising application with socio-economic and health impact in developing countries of arid climates is fog collection.[43–47] A recent report on climate change stated that there are 3.2 billion people around the world suffering from water shortage.[48] Fog water consists of micrometer-scale water droplets suspended in air. It is a vastly available and promising resource of uncontaminated drinking water in desert regions, coast and mountain areas.[49–51] To make use of fog for water supply, we designed a simple lab scale fog capture device, utilizing a container sealed by a Janus wood membrane (Fig. 4a). Fog capture devices were placed vertically and saturated fog was propelled horizontally toward the samples. The microscale fog droplets (~10 μm) first condensed on the membrane surface, and then grew and coalesced into larger droplets (~500 μm), and were finally transported by the Janus wood membrane to the container. After transport, the upper surface was released again and continued fog capturing.[52,53] For comparison, four fog collectors were fabricated, including a native wood membrane, hydrophobic wood membrane, Janus wood membrane in the positive direction, and Janus wood membrane in the reverse direction. Collected water increased steadily with fogging time for all samples. The native wood collector showed a relatively low fog capturing efficiency of 1.16 kg m^{-2} h^{-1} and the hydrophobic wood collector exhibited an even lower fog capturing efficiency of 0.61 kg m^{-2} h^{-1} because of the hydrophobic nature of the wood membrane. The dewing fog on the membrane surface could not penetrate through the membrane because of the absence of

Open Access Article. Published on 02 October 2020. Downloaded on 12/4/2025 8:07:59 PM.
This article is licensed under a Creative Commons Attribution 3.0 Unported Licence.

a wettability gradient, and slides away. The Janus wood collector in the positive direction, in contrast, revealed a greatly increased fog capture efficiency of 2.92 kg m^{-2} h^{-1}, 250% higher than that of native wood. The captured fog water on the Janus wood membrane in the positive direction was transported to a container driven by the wettability gradient, and simultaneously released the upper hydrophobic surface again. As a proof of the directional water transport properties, the Janus wood collector in the reverse direction showed a much lower efficiency of only 0.82 kg m^{-2} h^{-1}. The Janus wood membrane in the reverse direction absorbed a water film on the hydrophilic surface, but the water could not be transported. For practical applications, the durability of the Janus wood membranes is of utmost importance. Hence, we further evaluated the Janus wood collector regarding its cycling stability (Fig. 4b). The excellent fog collection efficiency of Janus wood membranes remained even after the cycling test for 10 cycles (96%), proving their outstanding stability and reusability.

Effective fog collecting devices require not only a high fog capture efficiency, but also a low water re-evaporation rate. In order to determine respective values a blank collector, a native wood collector and a Janus wood collector (in the positive direction) were placed in a thermostatic oven with temperature set at 25 °C, 45 °C, and 65 °C, and water evaporation rates were evaluated (Fig. 4c). The results showed that the water evaporation rate of the Janus wood collector was 48% lower than for the blank collector at 65 °C, significantly facilitating fog collection by a drastic reduction of the re-evaporation of preserved water. In short, our wood Janus membrane fog collector showed: (1) fast capture of fog water, (2) spontaneous transport of the captured water, (3) continuous release of the membrane surface, and (4) minimal re-evaporation rate of collected water. Based on these results, we envisage the utilization of Janus wood membranes as cost effective (Table S2, ESI†) fog collector devices in smart buildings as easily installable functional units (Fig. 4d). This proposed smart building solution could be highly promising for fog collection, especially in desert regions, with scarce liquid water but abundant fog water. Integrated in a bilayer, Janus wood membranes can capture fog water and autonomously transport the water into the water storing layer during humid nighttime.[54] The so harvested water is then ready for daily use.

Conclusions

In summary, we report here a mechanically robust bio-based and renewable Janus wood membrane, demonstrating directional, spontaneous, and fast transport of water. Profiting from its unique intrinsic porous structure of, wood serves as an ideal substrate for liquid transport. Native wood membranes were first hydrophobized with fluoro-oxysilane/TiO_2 nanoparticles, and then UV irradiated on one side to create the needed wettability gradient through the thickness of the Janus wood membrane. The reported Janus wood membrane exhibits an excellent liquid transport speed, even at a high membrane thickness, allowing circumventing the common limitations of comparable systems regarding the engineering application of Janus membranes. As an application concept, we proved the excellent fog capture efficiency of Janus wood membranes, exhibiting great potential for future smart buildings in arid areas.

Author contributions

Y. D. and T. K. conceived the study; Y. D. designed and carried out the experiments and characterization; Y. D. and T. K. co-wrote the manuscript. All the authors discussed the results and commented on the manuscript.

Data and materials availability

All data are available in the manuscript or the ESI† materials.

Conflicts of interest

There are no conflicts to declare.

Acknowledgements

Funding: The project was conducted in the framework of the SNF project "Hierarchical cellulose scaffolds for structural and functional gradient materials" (200021_184821/1).

References

1 H. A. Stone, A. D. Stroock and A. Ajdari, *Annu. Rev. Fluid. Mech.*, 2004, **36**, 381–411.
2 M. Abdelgawad and A. R. Wheeler, *Adv. Mater.*, 2009, **21**, 920–925.
3 M. Nosonovsky and B. Bhushan, *Curr. Opin. Colloid Interface Sci.*, 2009, **14**, 270–280.
4 T. S. Wong, S. H. Kang, S. K. Y. Tang, E. J. Smythe, B. D. Hatton, A. Grinthal and J. Aizenberg, *Nature*, 2011, **477**, 443–447.
5 T. M. Schutzius, S. Jung, T. Maitra, G. Graeber, M. Kohme and D. Poulikakos, *Nature*, 2015, **527**, 82–85.
6 Y. Zheng, H. Bai, Z. Huang, X. Tian, F.-Q. Nie, Y. Zhao, J. Zhai and L. Jiang, *Nature*, 2010, **463**, 640–643.
7 Y. Zheng, X. Gao and L. Jiang, *Soft Matter*, 2007, **3**, 178–182.
8 H. Bai, X. Tian, Y. Zheng, J. Ju, Y. Zhao and L. Jiang, *Adv. Mater.*, 2010, **22**, 5521–5525.
9 M. Du, Y. Zhao, Y. Tian, K. Li and L. Jiang, *Small*, 2016, **12**, 1000–1005.
10 C. Liu, J. Ju, Y. Zheng and L. Jiang, *ACS Nano*, 2014, **8**, 1321–1329.
11 J. Ju, K. Xiao, X. Yao, H. Bai and L. Jiang, *Adv. Mater.*, 2013, **25**, 5937–5942.
12 K. Yin, H. Du, X. Dong, C. Wang, J.-A. Duan and J. He, *Nanoscale*, 2017, **9**, 14620–14626.
13 J. R. Wu, K. Yin, L. M. Li, Z. P. Wu, S. Xiao, H. Wang, J. A. Duan and J. He, *Nanoscale*, 2020, **12**, 4077–4084.
14 K. Ichimura, S. K. Oh and M. Nakagawa, *Science*, 2000, **288**, 1624–1626.

Open Access Article. Published on 02 October 2020. Downloaded on 12/4/2025 8:07:59 PM.
This article is licensed under a Creative Commons Attribution 3.0 Unported Licence.

15 N. Bjelobrk, H. L. Girard, S. B. Subramanyam, H. M. Kwon, D. Quere and K. K. Varanasi, *Phys. Rev. Fluids*, 2016, **1**, 063902.
16 J. Vialetto, M. Hayakawa, N. Kavokine, M. Takinoue, S. N. Varanakkottu, S. Rudiuk, M. Anyfantakis, M. Morel and D. Baigl, *Angew. Chem., Int. Ed.*, 2017, **56**, 16565–16570.
17 H. Wang, J. Ding, L. Dai, X. Wang and T. Lin, *J. Mater. Chem.*, 2010, **20**, 7938–7940.
18 H. Zhou, H. Wang, H. Niu and T. Lin, *Sci. Rep.*, 2013, **3**, 6.
19 C. Zeng, H. Wang, H. Zhou and T. Lin, *Adv. Mater. Interfaces*, 2016, **3**, 7.
20 H. Wang, H. Zhou, X. Wei, H. Niu and T. Lin, *Adv. Mater. Interfaces*, 2018, **5**, 1800815.
21 J. Wu, H. Zhou, H. Wang, H. Shao, G. Yan and T. Lin, *Adv. Mater. Interfaces*, 2019, **6**, 1801529.
22 D. Miao, Z. Huang, X. Wang, J. Yu and B. Ding, *Small*, 2018, **14**, 10.
23 G. Huang, Y. Liang, J. Wang, X. Zeng, Z. Li and X. Zhang, *Mater. Lett.*, 2019, **246**, 76–79.
24 L. A. Berglund and I. Burgert, *Adv. Mater.*, 2018, **30**, 1704285.
25 T. Keplinger, X. Wang and I. Burgert, *J. Mater. Chem. A*, 2019, **7**, 2981–2992.
26 M. Vidiella del Blanco, E. J. Fischer and E. Cabane, *Adv. Mater. Interfaces*, 2017, **4**, 1700584.
27 F. Chen, A. S. Gong, M. Zhu, G. Chen, S. D. Lacey, F. Jiang, Y. Li, Y. Wang, J. Dai, Y. Yao, J. Song, B. Liu, K. Fu, S. Das and L. Hu, *ACS Nano*, 2017, **11**, 4275–4282.
28 Q. Fu, F. Ansari, Q. Zhou and L. A. Berglund, *ACS Nano*, 2018, **12**, 2222–2230.
29 Y. Q. Luo, F. Song, C. Xu, X. L. Wang and Y. Z. Wang, *Chem. Eng. J.*, 2020, 383.
30 C. Goldhahn, M. Schubert, T. Luthi, T. Keplinger, I. Burgert and M. Chanana, *ACS Sustainable Chem. Eng.*, 2020, **8**, 7205–7213.
31 K. F. Eid, M. Panth and A. D. Sommers, *Eur. J. Phys.*, 2018, **39**, 21.
32 H. Bai, L. Wang, J. Ju, R. Sun, Y. Zheng and L. Jiang, *Adv. Mater.*, 2014, **26**, 5025–5030.
33 X. Zhang, H. Kono, Z. Liu, S. Nishimoto, D. A. Tryk, T. Murakami, H. Sakai, M. Abe and A. Fujishima, *Chem. Commun.*, 2007, 4949–4951, DOI: 10.1039/b713432k.
34 Y. Q. Zhu, J. F. Shi, Q. Z. Huang, L. L. Wang and G. Xu, *Chem. Commun.*, 2017, **53**, 2363–2366.
35 S. Nishimoto, M. Becchaku, Y. Kameshima, Y. Shirosaki, S. Hayakawa, A. Osaka and M. Miyake, *Thin Solid Films*, 2014, **558**, 221–226.
36 T. Kanbayashi, Y. Kataoka, A. Ishikawa, M. Matsunaga, M. Kobayashi and M. J. J. o. W. S. Kiguchi, *J. Wood Sci.*, 2018, **64**, 169–172.
37 V. Jirous-Raikovic, H. Turkulin and E. R. Miller, *Surf. Coat. Int., Part B*, 2004, **87**, 241–247.
38 Y. Kataoka, M. Kiguchi, R. S. Williams and P. D. Evans, *Holzforschung*, 2007, **61**, 23–27.
39 M. El Khoury, K. Eyer, G. Chenon, L. Cayrefourcq, M. Mazel, J. Bibette, C. Alix-Panabieres and J. Baudry, *Clin. Exp. Metastasis*, 2018, **35**, 205.
40 X. Tian, J. Li and X. Wang, *Soft Matter*, 2012, **8**, 2633–2637.
41 M. K. Chaudhury and G. M. Whitesides, *Science*, 1992, **256**, 1539–1541.
42 F. Brochard, *Langmuir*, 1989, **5**, 432–438.
43 J. Ju, H. Bai, Y. M. Zheng, T. Y. Zhao, R. C. Fang and L. Jiang, *Nat. Commun.*, 2012, **3**, 6.
44 H. Kim, S. Yang, S. R. Rao, S. Narayanan, E. A. Kapustin, H. Furukawa, A. S. Umans, O. M. Yaghi and E. N. Wang, *Science*, 2017, **356**, 430.
45 M. Wang, Q. Liu, H. R. Zhang, C. Wang, L. Wang, B. X. Xiang, Y. T. Fan, C. F. Guo and S. C. Ruan, *ACS Appl. Mater. Interfaces*, 2017, **9**, 29248–29254.
46 R. J. Hu, N. Wang, L. L. Hou, Z. M. Cui, J. C. Liu, D. M. Li, Q. Z. Li, H. L. Zhang and Y. Zhao, *J. Mater. Chem. A*, 2019, **7**, 124–132.
47 P. S. Raux, S. Gravelle and J. Dumais, *Nat. Commun.*, 2020, **11**, 7.
48 W. H. Organization, *National Systems to Support Drinking-Water: Sanitation and Hygiene: Global Status Report 2019: UN-water Global Analysis and Assessment of Sanitation and Drinking-Water: GLAAS 2019 Report*, 2019, p. 144.
49 R. S. Schemenauer and P. Cereceda, *J. Appl. Meteorol.*, 1994, **33**, 1313–1322.
50 P. Gandhidasan and H. I. Abualhamayel, *Water Environ. J.*, 2007, **21**, 19–25.
51 O. Klemm, R. S. Schemenauer, A. Lummerich, P. Cereceda, V. Marzol, D. Corell, J. van Heerden, D. Reinhard, T. Gherezghiher, J. Olivier, P. Osses, J. Sarsour, E. Frost, M. J. Estrela, J. A. Valiente and G. M. Fessehaye, *Ambio*, 2012, **41**, 221–234.
52 J. Li, J. Li, J. Sun, S. Feng and Z. Wang, *Adv. Mater.*, 2019, **31**, 1806501.
53 M. Cao, J. Xiao, C. Yu, K. Li and L. Jiang, *Small*, 2015, **11**, 4379–4384.
54 M. Galun, *Handbook of Lichenology*, CRC Press, 2019.

 This journal is © The Royal Society of Chemistry 2020